NANO LETTERS

pubs.acs.org/NanoLett
Letter

Orientational Nanoconjugation with Gold Endows Marked Antimicrobial Potential and Drugability of Ultrashort Dipeptides

Zhiye Zhang,[¶] Yaoyao Chen,[¶] Jinai Gao,[¶] Min Yang,[¶] Dengdeng Zhang, Le Wang, Tianyu Zhang, Qiqi Cao, James Mwangi, Chenglu He, Ya Li, Xiangsheng Liu, Xingyu Jiang, Peter Muiruri Kamau, and Ren Lai*

Cite This: *Nano Lett.* 2023, 23, 11874−11883

Read Online

ACCESS | Metrics & More | Article Recommendations | Supporting Information

ABSTRACT: Antibiotic resistance is a global threat. Antimicrobial peptides (AMPs) are highly desirable to treat multidrug-resistant pathogen infection. However, few AMPs are clinically available, due to high cost, instability, and poor selectivity. Here, ultrashort AMPs (2−3 residues with an N-terminal cysteine) are designed and assembled as gold nanoparticles. Au−S conjugation and ultrashort size restrict nonspecific reactions and peptide orientation, thus concentrating positively charged residues on the surface. The nanostructured assemblies enormously enhance antimicrobial abilities by 1000−6000-fold and stability. One representative (Au-Cys-Arg-NH_2, Au_CR) shows selective antibacterial activity against *Staphylococcus aureus* with 10 nM minimal inhibitory concentration. Au_CR has comparable or better *in vivo* antimicrobial potency than vancomycin and methicillin, with low propensity to induce resistance, little side effects, and high stability (17.5 h plasma half-life). Au_CR acts by inducing collapse of membrane potential and rupture of the bacterial membrane. The report provides insights for developing AMP−metal nanohybrids, particularly tethering nonspecific reactions and AMP orientation on the metal surface.

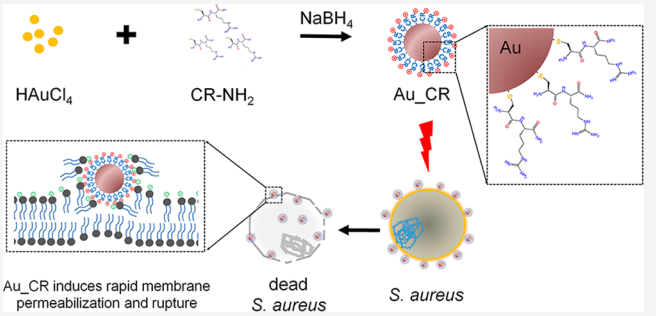

KEYWORDS: *dipeptide, gold nanoparticles, antibiotic-resistance, antimicrobial peptides*

The continued overuse of antibiotics has been accompanied by the rapid emergence of antibiotic-resistant bacteria.[1,2] According to a disturbing prediction by the World Health Organization (WHO), by the year 2050, 10 million deaths will be caused annually by drug-resistant infections.[3] Many problematic multidrug-resistant (MDR) bacteria are emerging, such as MDR *Pseudomonas aeruginosa*; vancomycin-resistant enterococci (VRE); methicillin-resistant *Staphylococcus aureus* (MRSA); vancomycin-resistant MRSA; carbapenem-resistant *Acinetobacter baumannii*, *Escherichia coli*, and *Klebsiella pneumoniae*; and extensively drug-resistant (XDR) *Mycobacterium tuberculosis*.[4,5] As an important opportunistic pathogen, *S. aureus* persistently colonizes about 20% of the human population and can cause both superficial and invasive, potentially life-threatening, infections such as sepsis, endocarditis, and pneumonia. MRSA is prevalent in hospitals, and hypervirulent MRSA strains are spreading throughout the community.[6−10]

Antimicrobial peptides (AMPs) show excellent potential for combating these threats due to their low tendency to select for resistance, rapid killing action, and desirable clinical efficacy against several MDR pathogens. However, several factors curtail their full utilization and approval for clinical application.[11−13] One of the limiting factors is AMPs' sensitivity to proteolytic digestion, and toxicity and efficacy of AMPs are other major drawbacks. Moreover, compared to conventional antibiotics, most druggable AMPs are expensive to produce. Therefore, current efforts are being directed at developing strategies to improve the efficacy of AMPs *in vivo*, design shorter peptides, enhance selectivity for microbial cells while reducing cytotoxicity, increase stability, and resist proteolytic degradation.[14] Chemical modifications such as the addition of D-amino acids, cyclization, or acetylation are important strategies to solve these issues.[14,15] However, additional modifications add to the production costs. Another possible strategy to improve the stability and efficacy of AMPs is the use of carrier delivery systems.[16] Of particular interest is the use of nanocarriers, which are designed and conjugate AMPs to prevent self-aggregation and improve chemical stability and release profiles of AMPs to target sites.[17−20]

Received: October 13, 2023
Revised: December 7, 2023
Accepted: December 7, 2023
Published: December 14, 2023

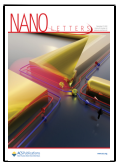

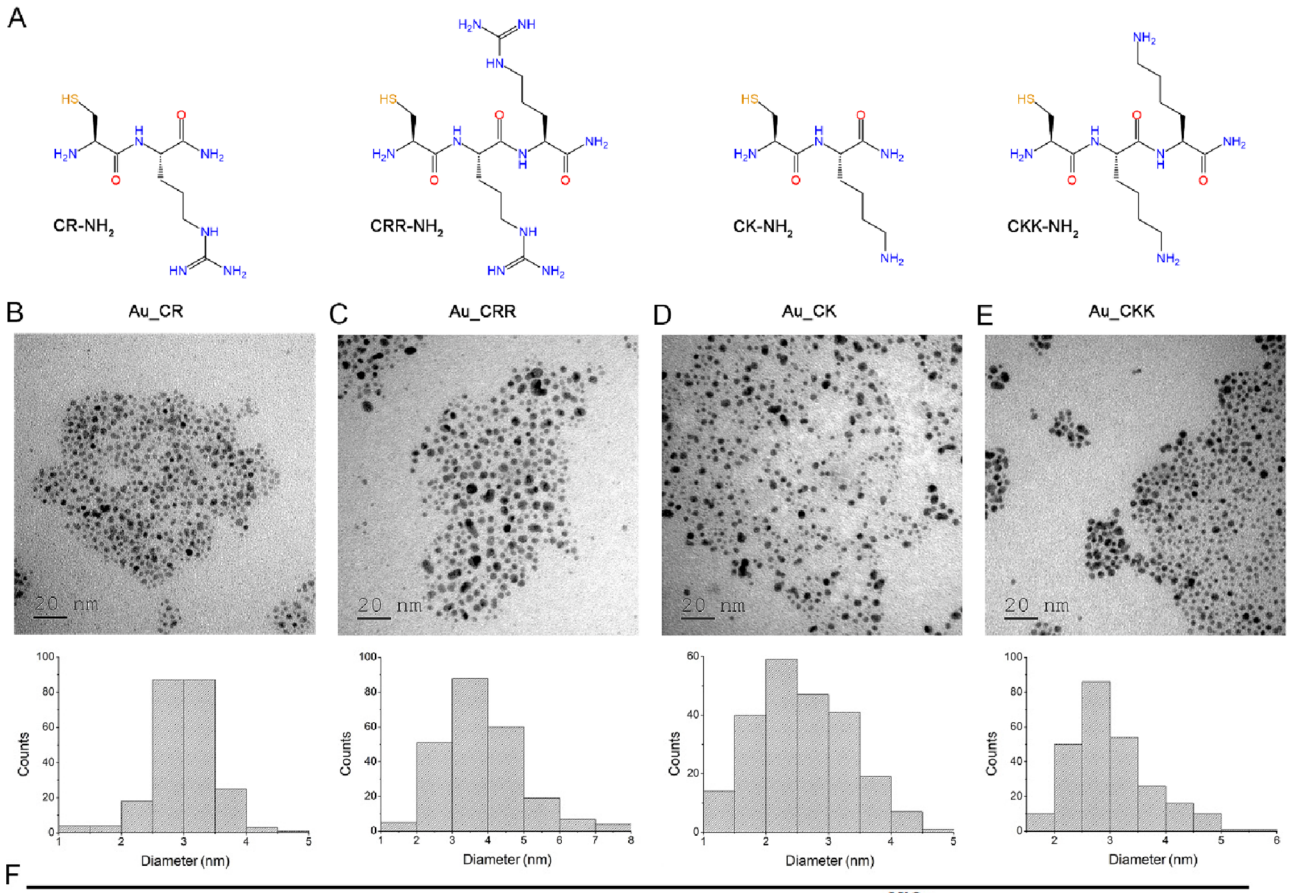

F

		MICs			
		E. coli	*B. subtilis*	*S. aureus*	*C. albicans*
Au_CR	Au weight (μg/mL)	> 100.00	> 100.00	1.56	> 100.00
	NP molar (μM)	> 0.61	> 0.61	0.01	> 0.61
	CR molar (μM)	> 234.52	> 234.52	3.66	> 234.52
	CR weight (μg/mL)	> 64.81	> 64.81	1.01	> 64.81
Au_CRR	Au weight (μg/mL)	> 100.00	> 100.00	6.25	> 100.00
	NP molar (μM)	> 0.31	> 0.31	0.02	> 0.31
	CRR molar (μM)	> 136.91	> 136.91	8.56	> 136.91
	CRR weight (μg/mL)	> 59.22	> 59.22	3.70	> 59.22
Au_CK	Au weight (μg/mL)	> 100.00	> 100.00	25.00	> 100.00
	NP molar (μM)	> 0.97	> 0.97	0.24	> 0.97
	CK molar (μM)	> 87.82	> 87.82	21.95	> 87.82
	CK weight (μg/mL)	> 21.81	> 21.81	5.45	> 21.81
Au_CKK	Au weight (μg/mL)	> 100.00	> 100.00	6.25	> 100.00
	NP molar (μM)	> 0.60	> 0.60	0.04	> 0.60
	CKK molar (μM)	> 243.90	> 243.90	15.24	> 243.90
	CKK weight (μg/mL)	> 91.83	> 91.83	5.74	> 91.83
CR, CRR, CK, or CKK	Molar (mM)	> 25	> 25	≥ 25	> 25

Figure 1. Characterizations of ultrashort peptide-conjugated gold nanoparticles and their antimicrobial activities. (A) Structural formulas of ultrashort peptides. TEM images of Au_CR (B), Au_CRR (C), Au_CK (D), and Au_CKK (E) (top), with diameters of 3.0 ± 0.5 nm, 3.8 ± 1.0 nm, 2.6 ± 0.7 nm, and 3.0 ± 0.7 nm, respectively (bottom). (F) Antimicrobial activities of Au_CR, Au_CRR, Au_CK, and Au_CKK and their corresponding free peptides against *E. coli*, *B. subtilis*, *S. aureus*, and *C. albicans*. MICs are shown in weight (μg/mL) and molar (μM) concentrations. MICs represent mean values of three independent experiment.

Gold nanoparticles (NPs) are comparatively safer than other metallic NPs due to the inert and nontoxic nature of gold and high biocompatibility.[21,22] In this study, we aim to develop novel antibacterial agents by designing a series of ultrashort AMPs (2−3 residues) and engineering them to conjugate with gold NPs by a one-step strategy. The formulation reported here may be useful as a general platform to develop innovative antibacterial agents.

Peptides have multiple functional groups, including amino and thiol groups, which can immobilize peptides onto gold NPs by electrostatic interaction and Au−S coordinate covalent bonds, respectively.[17,23,24] Given that covalent conjugation is reliable and conjugates show high quality and homogeneity, we designed short peptides with an N-terminal cysteine, allowing them to conjugate to gold via Au−S bond formation. To avoid nonspecific reactions with AMP side-chain amino groups that affect peptide orientation on the surface of gold to possibly decrease antimicrobial activity, we restricted the length of peptides to no more than 3 amino acid residues. In addition, a net positive charge (provided by Lys/Arg) of peptide is necessary because the cationic properties of AMPs are highly associated with their antimicrobial activity.[25] To meet the requirements mentioned above, six short peptides with an amidated C terminus to improve stability and reduce negative charges, including Cys-Arg-NH_2 (CR), Cys-Lys-NH_2 (CK), Cys-Arg-Arg-NH_2 (CRR), Cys-Lys-Lys-NH_2 (CKK) (Figure

https://doi.org/10.1021/acs.nanolett.3c03909
Nano Lett. 2023, 23, 11874−11883

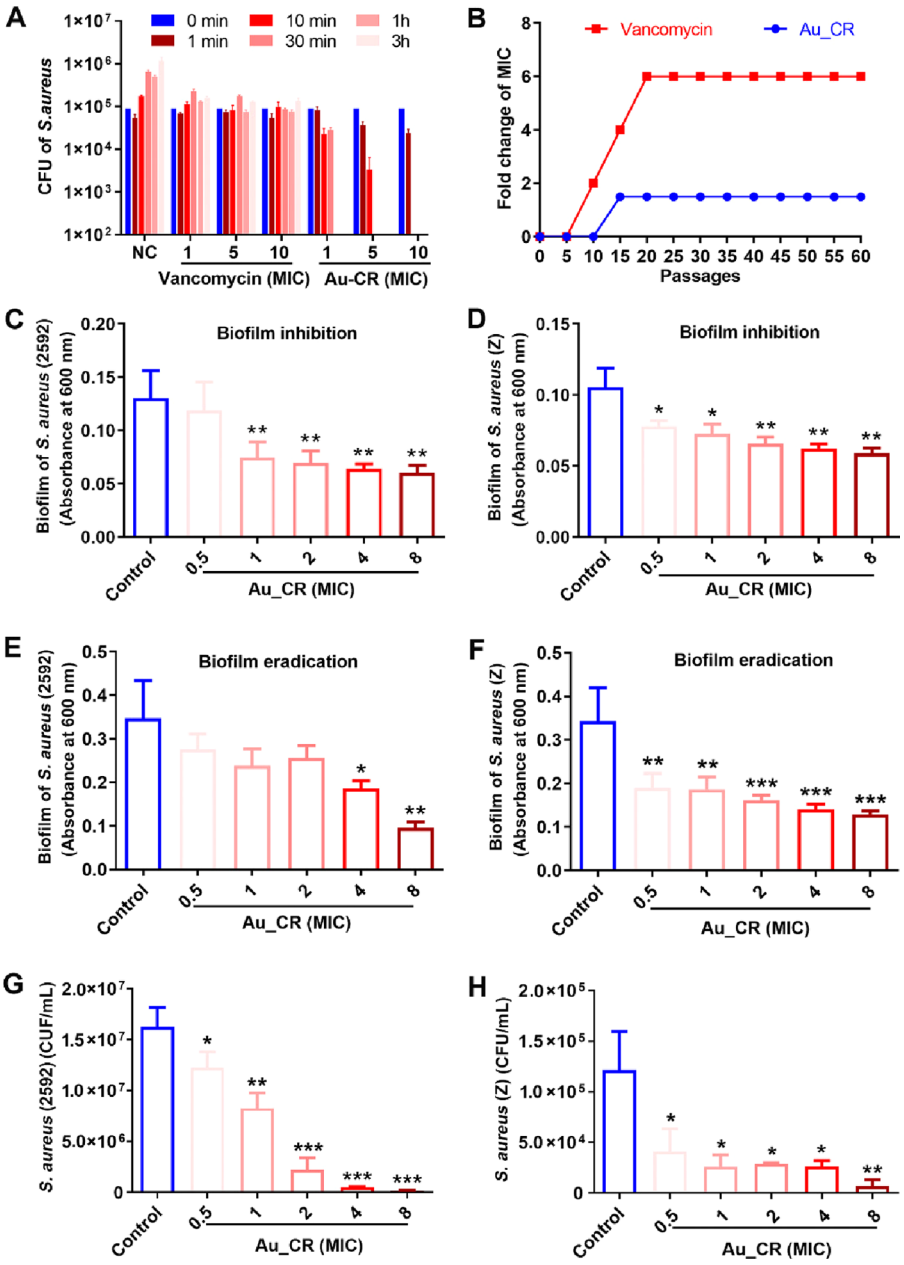

Figure 2. Au_CR shows rapid killing effect, low propensity to induce resistance, and potent effects to kill biofilm and persister cells. (A) Killing kinetics of Au_CR against *S. aureus*. (B) Resistance development of *S. aureus* following long-term exposure (60 passages) to Au_CR or vancomycin. Inhibitory effects of Au_CR on biofilm formation of *S. aureus* ATCC2592 (C) and Z (D, clinically isolated strain). Effects of Au_CR on established biofilm eradication of *S. aureus* ATCC2592 (E) and Z (F). Bactericidal activities of Au_CR against persister cells of *S. aureus* ATCC2592 (G) and Z (H). Data represent means ± SD of three individual experiments. *$p < 0.05$, **$p < 0.01$, and ***$p < 0.001$; one-way ANOVA with Dunnett *post hoc* test compared with control (PBS).

1A), Cys-Arg-Lys-NH_2 (CRK), and Cys-Lys-Arg-NH_2 (CKR), were designed.

The NPs were assembled by short peptides, which were conjugated with gold via the reduction of $HAuCl_4$ by $NaBH_4$ in the presence of short peptides in methanol. Based on transmission electron microscopy (TEM) and statistical analysis, the diameters of the CR-gold (Au_CR), CRR-gold (Au_CRR), CK-gold (Au_CK), and CKK-gold NPs (Au_CKK) were 3.0 ± 0.5, 3.8 ± 1.0, 2.6 ± 0.7, and 3.0 ± 0.7 nm, respectively (Figure 1B–E). The corresponding ultraviolet–visible (UV–vis) absorption spectra of the short peptides and peptide-conjugated gold NPs are shown in Figure S1. A broadened peak appeared at ∼535 nm for the peptide-conjugated gold NPs, which was possibly due to their small size, and the plasmon peak was not evident on the absorbance spectra, consistent with previous findings.[26] X-ray photoelectron spectroscopy (XPS) demonstrated that the molar ratios of S to Au in Au_CR, Au_CRR, Au_CK, and Au_CKK were 0.46:1, 0.27:1, 0.17:1, and 0.48:1, respectively (Figure S2 and Table S1). The numbers of CR, CRR, CK, and CKK on each gold NP were 383, 448, 91, and 406, respectively (Table S1). The zeta potentials showed that all four peptide-conjugated gold NPs were positively charged (Table S1). Although Au_CRR and Au_CKK had one more amino group than Au_CR, the zeta potentials of them were lower than Au_CR, maybe because the slight reaction between the side

https://doi.org/10.1021/acs.nanolett.3c03909
Nano Lett. 2023, 23, 11874−11883

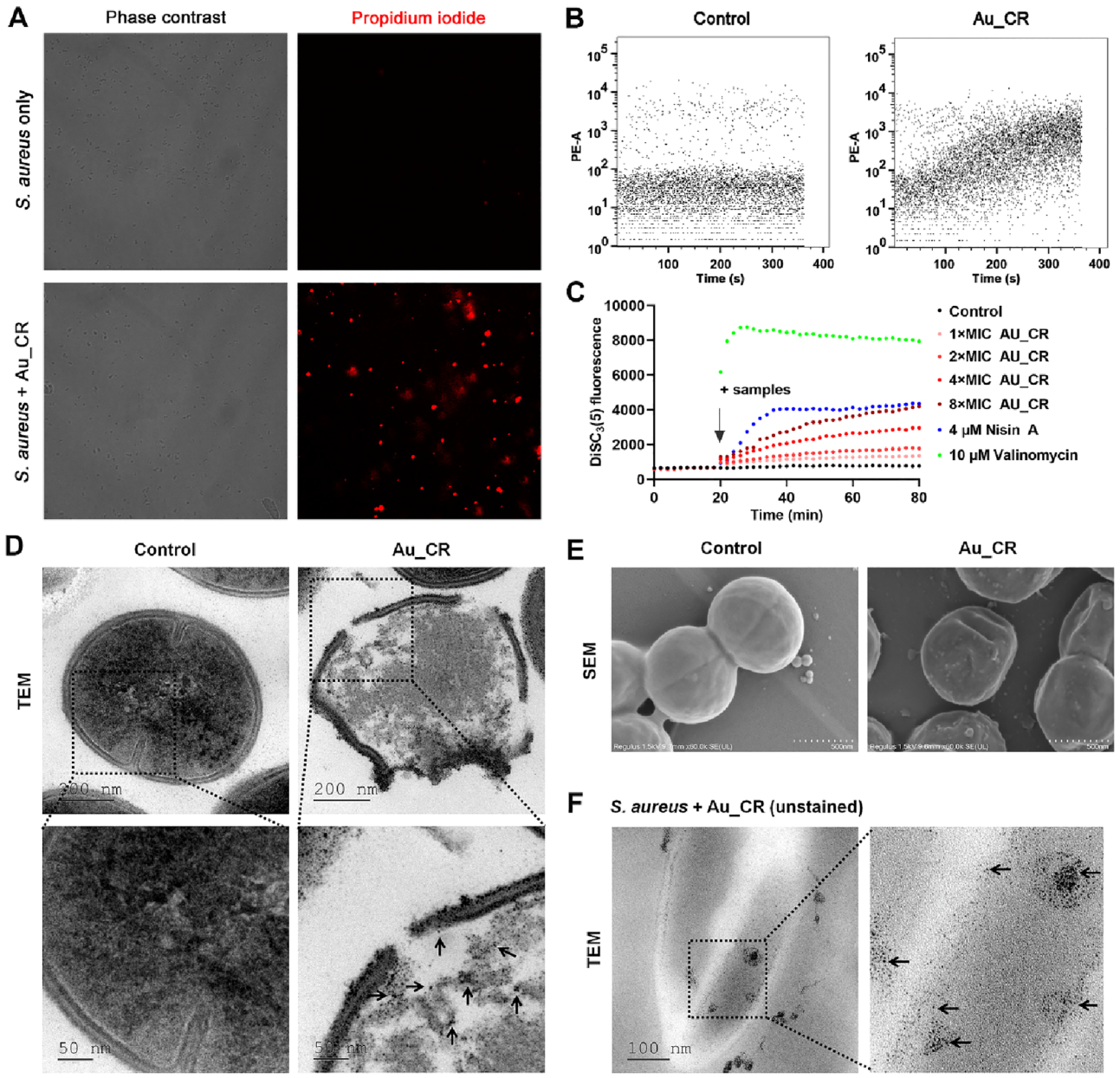

Figure 3. Au_CR induces rapid membrane permeabilization and rupture. (A) Fluorescence assay of *S. aureus* treated with Au_CR (5 × MIC) by PI staining. Image of corresponding fluorescence (right) in phase contrast mode is shown (left). (B) Kinetics of PI influx in *S. aureus*. *S. aureus* cells were first incubated with PI for 15 min, then measured by flow cytometry in the presence or absence of Au_CR (5 × MIC) for 6 min. Images are representative of at least three independent experiments. (C) Membrane potential levels of *S. aureus* upon addition of Au_CR (1−8 × MIC), Nisin A (4 μM), and Valinomycin (10 μM). Saline was used as control. TEM (D) and SEM (E) images showing morphological changes in *S. aureus* treated with Au_CR (5 × MIC, 7.8 μg/mL) or without Au_CR (Control). (F) TEM image of unstained super thin slices of *S. aureus* treated with Au_CR (5 × MIC) showing the internalized NPs. The graph depicts a representative measurement of three independent replicates. In panels D and F, the arrows indicate the NPs.

chain amino groups and surface of gold NPs decreased their zeta potentials. Au_CRK and Au_CKR were not focused on in this work since they showed relatively weak antimicrobial functions.

We next evaluated the antimicrobial properties of peptide-conjugated gold NPs *in vitro*. As illustrated in Figure 1F, the free peptides showed extremely weak antimicrobial effects (minimal inhibitory concentrations (MICs) ≥ 25 mM; i.e., ≥6 200 μg/mL). However, after conjugation with gold, they exhibited significant antimicrobial activities against *S. aureus*, with MICs of 1.56, 6.25, 25.00, and 6.25 μg/mL for Au_CR, Au_CRR, Au_CK, and Au_CKK, respectively (Figure 1F). They showed weak antimicrobial activities against *E. coli*, *Bacillus subtilis*, or *Candida albicans* (MICs > 100 μg/mL). To further assess their antimicrobial effects, we tested their antimicrobial properties against 19 clinically isolated *S. aureus* strains. Remarkably, Au_CR also showed the highest antibacterial activity against the clinical *S. aureus* strains, with MICs from 1.56 to 4.69 μg/mL (Table S2). Similarly, Au_CRR, Au_CK, and Au_CKK showed potent activities against these strains, with MICs between 6.25 and 12.50 μg/mL, 12.50 and 37.5 μg/mL, and 6.25 and 12.50 μg/mL (20−240 nM), respectively. Additionally, we also tested the antimicrobial activities of methicillin and vancomycin against

https://doi.org/10.1021/acs.nanolett.3c03909
Nano Lett. 2023, 23, 11874−11883

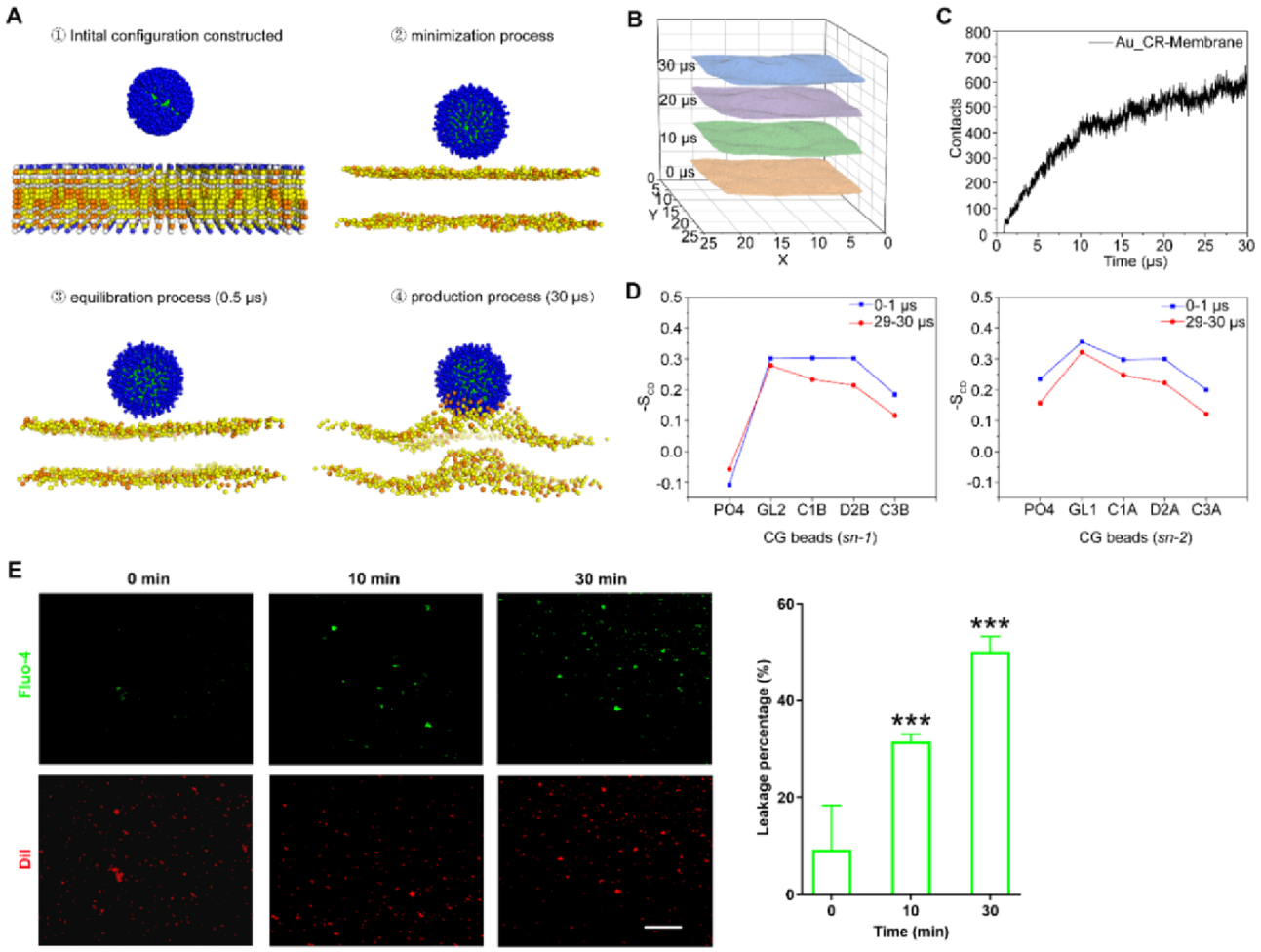

Figure 4. Au_CR interacts with and disrupts mimetic membrane. (A) The process of Au_CR particle penetrating into the model membrane in MD simulations. The Cys residues in Au_CR are shown as green spheres, and Arg residues are shown as blue spheres. The phospholipids are represented by PO4 beads for convenience. The yellow spheres represent the DOPC molecules, and the orange spheres represent DOPG molecules. (B) The simulation snapshots with an interval of 10 μs of the model membrane interface with the influence of Au_CR nanoparticle. (C) The number of contacts between Au_CR and membrane during MD simulations. (D) Deuterium order parameter results for lipid chains within 0.5 nm near the particle during first and last 1 μs simulation. The first 1 μs is colored in blue and last 1 μs in red. (E) Fluorescence assay of liposomes labeled with DiI (red) and encapsulated Fluo-4 (green) in a solution containing 10 mM Ca^{2+} and 5 × MIC Au_CR. The images were captured after 0, 10, and 30 min of incubation with Au_CR (left). Percentage of leaked vesicles was also analyzed (right). Scale bar: 50 μm. ***$p < 0.01$, one-way ANOVA with Dunnett *post hoc* test compared with 0 min group. Images are representative of at least three independent experiments.

these clinical strains (Table S2). Nine strains (47.4%) showed obvious methicillin resistance, with MICs of 2.34−200 μg/mL (4−339-fold increase in MICs). Vancomycin also showed antibacterial effects against most of the clinically isolated *S. aureus* strains (MICs of 1.17−2.34 μg/mL), with only four isolates (21.1%) exhibiting a 2-fold increase in their MICs (2.34 μg/mL).

Cationic peptides usually show a certain level of hemolysis and/or cytotoxicity near their therapeutic concentrations, which greatly impedes their clinical use as therapeutics.[2,27] To understand the potential toxicity of peptide-conjugated gold NPs, we next evaluated their hemolytic and cytotoxic activities. Notably, at a high concentration of 100 μg/mL (64-fold higher than the Au_CR MIC against standard *S. aureus*), the four gold NPs exhibited negligible hemolytic activity (less than 3% hemolysis, Figure S3). We also tested their cytotoxicity against human HaCaT keratinocyte cells and human umbilical vein endothelial cells (HUVECs). As illustrated in Figure S4, Au_CR showed little effect on cell viability, and Au_CRR, Au_CK, and Au_CKK exerted a moderate degree of cytotoxicity. Thus, Au_CR showed the highest antibacterial activity and negligible toxicity, suggesting high potential as an ideal antimicrobial candidate.

We next determined the killing kinetics of Au_CR against *S. aureus*. As shown in Figure 2A, Au_CR showed rapid and dose-dependent killing effects, with complete *S. aureus* death within 60 min at 1 × MIC, 30 min at 5 × MIC, and 10 min at 10 × MIC. In contrast, vancomycin could not kill *S. aureus* within 3 h, even at 10 × MIC. This may be because vancomycin only inhibited bacterial cell wall synthesis without killing the bacteria within the tested time (3 h). As Au_CR killed *S. aureus* quickly, bacteria may have difficulty developing resistance. We therefore evaluated the selection of resistance through serial passaging (up to 60 passages) in the presence of varied concentrations of Au_CR or vancomycin. As shown in Figure 2B, *S. aureus* did not easily develop resistance to Au_CR, and the MIC increased only 1.5-fold after 60 passages. However, exposure to vancomycin resulted in the rapid development of resistance after the first five passages and led to a 6-fold increase in the MIC after 20 passages. Collectively,

https://doi.org/10.1021/acs.nanolett.3c03909
Nano Lett. 2023, 23, 11874−11883

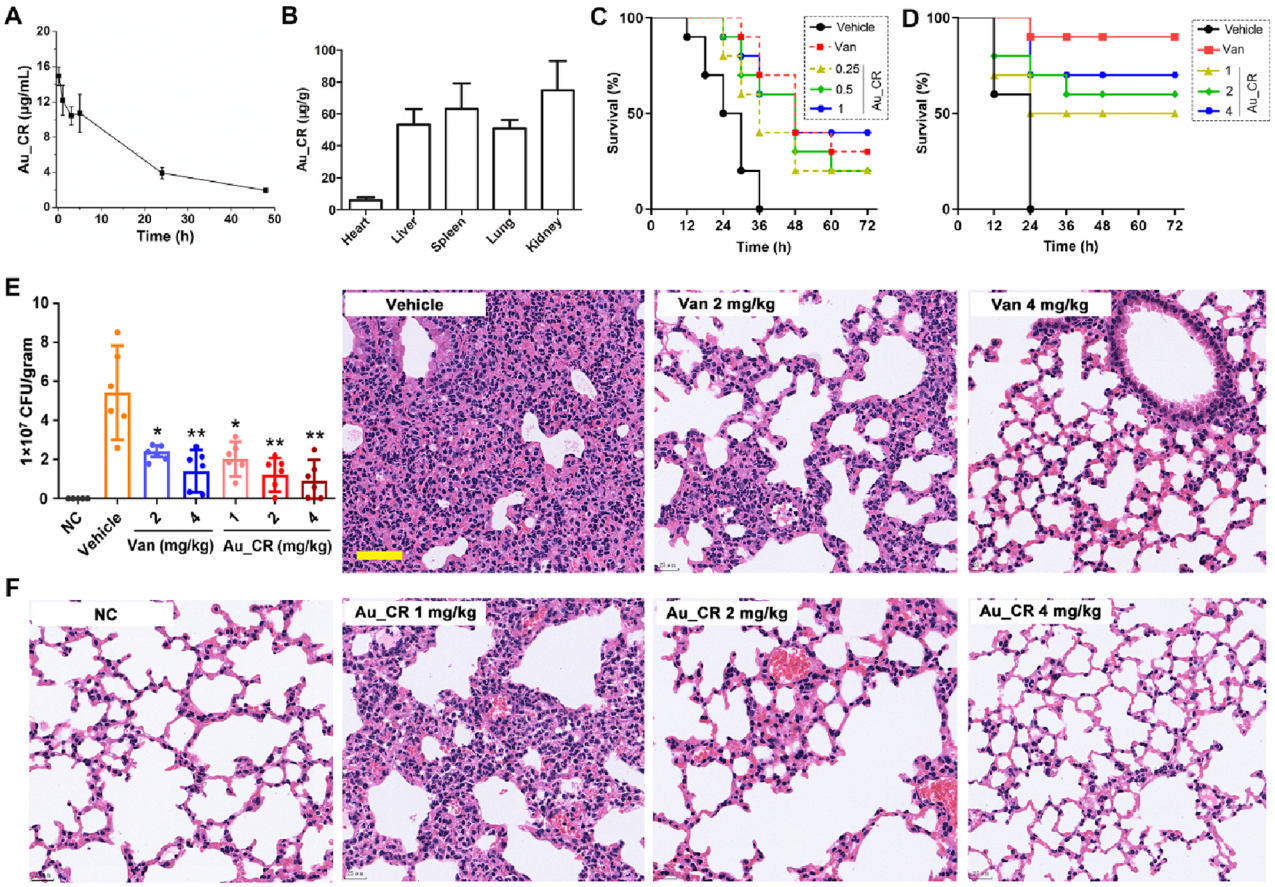

Figure 5. Au_CR increases survival and inhibits *S. aureus* lung infection and inflammation. (A) Pharmacokinetic profile of Au_CR via intravenous injection at Au dose of 10 mg/kg. (B) Biodistribution of Au_CR in main organs 48 h after injection. (C) Survival curves for mice (n = 10) after iv infection with *S. aureus* Z. Treatment with Au_CR (0.25, 0.5, and 1 mg/kg) and vancomycin (1 mg/kg) was performed (via iv injection) at 1 and 6 h after inoculation. (D) Survival curves for mice (n = 10) after ip infection with *S. aureus* Z and ip administration of Au_CR (1, 2, and 4 mg/kg) and vancomycin (4 mg/kg) at 1 and 6 h after infection. (E) Mice (n = 6) were first intranasally administered with *S. aureus* Z (clinically isolated strain), followed by iv treatment with Au_CR (1, 2, 4 mg/kg) or vancomycin (2 and 4 mg/kg) to examine their therapeutic effects, with bacterial load in lung homogenate shown. (F) Representative histopathological images of processed lung section with H&E staining. Scale bar represents 50 μm. Mouse model experiments were repeated twice. *p < 0.05 and **p < 0.01, two-way ANOVA with Dunnett *post hoc* test compared with vehicle group (sterile saline). Data in panels A, B, and E represent mean ± SD values of three independent experiments.

these results suggest that Au_CR exhibits rapid and potent bactericidal effects with a low propensity to induce resistance.

Pathogenic biofilms are formed by a thick and dense extracellular matrix, which can prevent antimicrobial agents from contacting the cells, thus contributing to drug resistance.[28,29] Thus, we next investigated the effects of Au_CR on antibiofilm formation and eradication. Notably, Au_CR inhibited the biofilm formation of the standard (Figure 2C) and clinically isolated (Figure 2D) *S. aureus* strains in a dose-dependent manner. Once formed, biofilms are very difficult to eradicate, resulting in chronic and persistent infections.[30] Interestingly, the preformed *S. aureus* biofilms were eliminated by Au_CR in a dose-dependent manner (Figure 2E,F).

All bacteria can form persisters, a drug-tolerant subpopulation of dormant cells, which have been implicated in biofilms and in chronic and recurrent infections.[31,32] As illustrated in Figure 2G,H, Au_CR showed potent killing effects against *S. aureus* persisters, even at a low concentration of 0.5 × MIC. More than half of the persister cells of the standard (Figure 2G) and clinical (Figure 2H) *S. aureus* strains were eliminated by 1 × MIC of Au_CR. Thus, together, the effects of Au_CR make it a promising antibiofilm and antipersister agent.

To elucidate a potential mechanism of action of Au_CR, effects of Au_CR on bacterial membrane permeabilization were studied by a fluorescence assay and flow cytometry. Compared to free *S. aureus* cells, 5 × MIC of Au_CR treatment for 30 min resulted in a significant increase in the number of fluorescent deposits (red), i.e., propidium iodide (PI) uptake (Figure 3A), indicating that Au_CR caused rapid membrane permeabilization. Furthermore, flow cytometry also detected immediate and increasing PI influx after Au_CR was added to the *S. aureus* cells (Figure 3B), further suggesting that Au_CR permeabilized the bacterial membrane quickly and in a time-dependent manner. Membrane permeabilization or collapse of membrane integrity may result from loss of membrane potential (or membrane electric potential, $\Delta\Psi$).[33] To test this hypothesis, we used the fluorescent dye 3,3-dipropylthiadicarbocyanine iodide ($DiSC_3(5)$) to evaluate whether Au_CR dissipated the membrane potential. As shown in Figure 3C, Au_CR gradually increased the fluorescence intensity of $DiSC_3(5)$ in a dose-dependent manner, indicating a gradual collapse of the membrane

https://doi.org/10.1021/acs.nanolett.3c03909
Nano Lett. 2023, 23, 11874−11883

potential after Au_CR treatment. The pore-forming lantibiotic Nisin A also caused a similar $DiSC_3(5)$ signal profile as Au_CR, but the effect was a little faster. The potassium ionophore valinomycin was also added as a control, which instantly dissipated the membrane potential (Figure 3C).

Membrane permeabilization may lead to disruption of the bacterial membrane structure. TEM images showed that the plasma membrane of *S. aureus* ruptured after Au_CR treatment, thus allowing entry of the NPs (Figure 3D). In contrast, the membranes of the untreated cells remained intact. The scanning electron microscopy (SEM) images also showed membrane rupture and pore formation in Au_CR-treated *S. aureus* cells (Figure 3E). TEM images of unstained slices further proved that Au_CR killed *S. aureus* by disrupting the bacterial membrane, with the NPs clearly internalized in the cytoplasm of the damaged *S. aureus* cells (Figure 3F). Together, these data demonstrate that Au_CR induces collapse of membrane potential and rupture of the bacterial membrane.

To further assess the possible antimicrobial mechanism of Au_CR, we performed all-atom (AA) and coarse-grained (CG) molecular dynamics (MD) simulations. After the construction of the AA model, the 3 nm gold core was coated with monolayer CR peptides by Au−S bonds. CR peptides were concentrated and evenly distributed on the gold surface. Guanidyl groups of arginine contributed positive charges orderly extended toward the outside (Figure S5A,B). The model of 1,2-dioleoyl-*sn*-glycerol-3-phosphocholine (DOPC) and 1,2-dioleoyl-*sn*-glycero-3-phospho-(1′-rac-glycerol) (DOPG) with a ratio of 7:3 was used to simulate negatively charged *S. aureus* membranes.[34,35] The root-mean-square deviation (RMSD) of Au_CR reached a steady state, ensuring structural stability in the later stage of MD simulations (Figure S5C). As shown in Figure 4A, once the simulation started, the Au_CR particles began to move toward the membrane quickly. In the production process, the lipid membrane became rough and formed a hump in another direction to accommodate the penetration of the particle. The phospholipids near the Au_CR particle became disordered, especially the DOPG molecules. The coordinates of PO4 beads in one side within 0.5 nm of the particle were extracted to depict the interface of the model membrane with the influence of the Au_CR particle (Figure 4B). With the penetration of the Au_CR particle, the membrane became bumpier. The contact curve demonstrated effective interactions between the Au_CR particle and membranes (Figure 4C). The deuterium order parameters were defined in a previous study to characterize the lipid order during simulation,[36] which are calculated for the angles between the bond vectors of two consecutive tail beads and the bilayer normal for the lipid acyl chains. The first and the last 1 μs production trajectory was used for deuterium order parameter analysis, and two lipid acyl chains (*sn*-1 and *sn*-2) were analyzed. Comparing the results before and after the simulations, the lipids near the particle become more disorderly as the simulation goes on (Figure 4D). Some lipids bent out the bilayer, and their deuterium order parameters decreased, further indicating the disturbance of the membrane induced by Au_CR.

We further investigated the effects of Au_CR on biomembrane-mimicking unilamellar vesicles, which were constructed using DOPC/DOPG lipids at a 7:3 ratio, as in the MD simulations. The vesicles were labeled with DiI (red) and preloaded with Fluo-4 (green), a Ca^{2+}-sensitive fluorescent dye, the fluorescence signal of which will be enhanced in the presence of Ca^{2+}. As illustrated in Figure 4E, 10 and 30 min after addition of Au_CR *in situ*, Fluo-4 fluorescent spots were significantly increased in a time-dependent manner, indicating that Au_CR induces liposome leakage and transmembrane influx of Ca^{2+}. Together, these data suggest Au_CR interacts with and disrupts the bacterial membrane.

Before we started to evaluate the therapeutic potential of Au_CR *in vivo*, metabolic stability and acute toxicity of it were first determined. As illustrated in Table S3, the incubation of Au_CR with plasma at 37 °C for 24 h had no apparent effect on its antibacterial activity against *S. aureus*, indicating its high plasma stability. Furthermore, pharmacokinetic analysis of Au_CR demonstrated a half-life of ∼17.5 h after intravenous (iv) injection into mice (Figure 5A and Figure S6). The injected Au_CR was predominantly localized in the kidneys, spleen, liver, and lungs with little found in the heart (Figure 5B). The high concentration of Au_CR in the kidneys indicated that it may be partially excreted via renal clearance, which is likely due to their small hydrodynamic size as smaller NPs show quicker renal clearance.[37] Importantly, after administration of Au_CR at a dose of 20 or 30 mg/kg, mice showed no signs of toxicity (Figure S7), suggesting the high biocompatibility of Au_CR *in vivo*.

We first investigated whether it would rescue C57BL/6 mice infected with a lethal dose of *S. aureus*. As shown in Figure 5C, Au_CR treatment via iv administration significantly increased the survival of mice after iv infection with a clinically isolated *S. aureus* strain (Z). Survival of Au_CR-treated mice after peritoneal infection with *S. aureus* was also significantly higher than that of vehicle (saline)-treated mice, and treatment with Au_CR had a dose-dependent impact on the survival rate (Figure 5D).

We next used MDR *S. aureus*-induced lung infection and bacteremia models to evaluate the therapeutic potential of Au_CR. In the first set of experiments, C57BL/6 mice were administered intranasally with a suspension of a clinically isolated *S. aureus* strain (Z) to induce lung infection, followed by iv treatment with Au_CR and control samples (vehicle and vancomycin). Notably, treatment with 1, 2, and 4 mg/kg Au_CR inhibited the bacterial load in the lung by 62.7%, 77.5%, and 83.0%, while 2 and 4 mg/kg vancomycin inhibited the bacterial load by 55.1% and 74.0%, respectively (Figure 5E). Au_CR demonstrated better therapeutic potential than vancomycin. Furthermore, histopathological examination of fixed lung sections revealed that Au_CR administration significantly alleviated lung inflammation and inflammatory cell infiltration (Figure 5F), indicating a potential anti-inflammatory effect *in vivo*.

In the second set of experiments, mice were inoculated with *S. aureus* Z via intraperitoneal (ip) injection, with Au_CR and controls also administered via ip injection to assess their effects on dissemination of bacteria from the peritoneal cavity to the blood, lung, liver, and spleen. As illustrated in Figure S8A,D, compared to the vehicle treatment, Au_CR treatment significantly suppressed (2−5-fold) bacterial dissemination to the blood and organs. Similar results were observed after treatment with vancomycin. In addition, *S. aureus* infection led to elevated cytokine levels of interleukin (IL)-1β, IL-6, IL-10, tumor necrosis factor (TNF)-α, monocyte chemotactic protein (MCP)-1, and interferon (IFN)-γ (Figure S8E−J). However, Au_CR treatment significantly suppressed these cytokine releases, further suggesting an anti-inflammatory potential of

https://doi.org/10.1021/acs.nanolett.3c03909
Nano Lett. 2023, 23, 11874−11883

Au_CR. Moreover, histopathological analysis of the lungs, liver, and spleen also highlighted the potent therapeutic effects of Au_CR against *S. aureus* dissemination *in vivo* (Figure S8K–M). Collectively, these results indicate that Au_CR can inhibit *S. aureus* infection and dissemination to target organs.

Collectively, our results indicated that the dipeptide (CR)-gold NPs exhibited highly potent bactericidal activity and specificity against *S. aureus* with a favorable safety profile and showed impressive therapeutic efficacy. The formulation reported here may be useful as a general platform to develop innovative antibacterial agents.

■ ASSOCIATED CONTENT

Supporting Information

The Supporting Information is available free of charge at https://pubs.acs.org/doi/10.1021/acs.nanolett.3c03909.

Materials, synthesis and characterization of nanoparticles, antimicrobial properties *in vitro* and *in vivo*, simulation setup and experimental procedures for pharmacokinetics and biodistribution study, Figures S1–S8, Tables S1–S3, and supplementary references (PDF)

■ AUTHOR INFORMATION

Corresponding Author

Ren Lai − *Engineering Laboratory of Peptides of Chinese Academy of Sciences, Key Laboratory of Bioactive Peptides of Yunnan Province, KIZ-CUHK Joint Laboratory of Bioresources and Molecular Research in Common Diseases, National Resource Center for Non-Human Primates, National Research Facility for Phenotypic & Genetic Analysis of Model Animals (Primate Facility), and Sino-African Joint Research Center, New Cornerstone Science Institute, Kunming Institute of Zoology, Chinese Academy of Sciences, Kunming, Yunnan 650223, China; School of Molecular Medicine, Hangzhou Institute for Advanced Study, University of Chinese Academy of Sciences, Hangzhou 310024 Zhejiang, China;* orcid.org/0000-0002-3123-2336; Email: rlai@mail.kiz.ac.cn

Authors

Zhiye Zhang − *Engineering Laboratory of Peptides of Chinese Academy of Sciences, Key Laboratory of Bioactive Peptides of Yunnan Province, KIZ-CUHK Joint Laboratory of Bioresources and Molecular Research in Common Diseases, National Resource Center for Non-Human Primates, National Research Facility for Phenotypic & Genetic Analysis of Model Animals (Primate Facility), and Sino-African Joint Research Center, New Cornerstone Science Institute, Kunming Institute of Zoology, Chinese Academy of Sciences, Kunming, Yunnan 650223, China;* orcid.org/0000-0002-1661-2277

Yaoyao Chen − *Department of Zoology, College of Life Sciences, Nanjing Agricultural University, Nanjing 210095 Jiangsu, China*

Jinai Gao − *Engineering Laboratory of Peptides of Chinese Academy of Sciences, Key Laboratory of Bioactive Peptides of Yunnan Province, KIZ-CUHK Joint Laboratory of Bioresources and Molecular Research in Common Diseases, National Resource Center for Non-Human Primates, National Research Facility for Phenotypic & Genetic Analysis of Model Animals (Primate Facility), and Sino-African Joint Research Center, New Cornerstone Science Institute, Kunming Institute of Zoology, Chinese Academy of Sciences, Kunming, Yunnan 650223, China; School of Molecular Medicine, Hangzhou Institute for Advanced Study, University of Chinese Academy of Sciences, Hangzhou 310024 Zhejiang, China*

Min Yang − *Engineering Laboratory of Peptides of Chinese Academy of Sciences, Key Laboratory of Bioactive Peptides of Yunnan Province, KIZ-CUHK Joint Laboratory of Bioresources and Molecular Research in Common Diseases, National Resource Center for Non-Human Primates, National Research Facility for Phenotypic & Genetic Analysis of Model Animals (Primate Facility), and Sino-African Joint Research Center, New Cornerstone Science Institute, Kunming Institute of Zoology, Chinese Academy of Sciences, Kunming, Yunnan 650223, China; Kunming College of Life Science, University of Chinese Academy of Sciences, Kunming 650204 Yunnan, China*

Dengdeng Zhang − *Engineering Laboratory of Peptides of Chinese Academy of Sciences, Key Laboratory of Bioactive Peptides of Yunnan Province, KIZ-CUHK Joint Laboratory of Bioresources and Molecular Research in Common Diseases, National Resource Center for Non-Human Primates, National Research Facility for Phenotypic & Genetic Analysis of Model Animals (Primate Facility), and Sino-African Joint Research Center, New Cornerstone Science Institute, Kunming Institute of Zoology, Chinese Academy of Sciences, Kunming, Yunnan 650223, China; Department of Pharmaceutical Sciences, College of Pharmaceutical Sciences, Soochow University, Suzhou 215123 Jiangsu, China*

Le Wang − *Department of Biomedical Engineering, Southern University of Science and Technology, Shenzhen 518055 Guangdong, China*

Tianyu Zhang − *Zhejiang Cancer Hospital, Hangzhou Institute of Medicine (HIM), Chinese Academy of Sciences, Hangzhou 310022 Zhejiang, China*

Qiqi Cao − *Department of Zoology, College of Life Sciences, Nanjing Agricultural University, Nanjing 210095 Jiangsu, China*

James Mwangi − *Engineering Laboratory of Peptides of Chinese Academy of Sciences, Key Laboratory of Bioactive Peptides of Yunnan Province, KIZ-CUHK Joint Laboratory of Bioresources and Molecular Research in Common Diseases, National Resource Center for Non-Human Primates, National Research Facility for Phenotypic & Genetic Analysis of Model Animals (Primate Facility), and Sino-African Joint Research Center, New Cornerstone Science Institute, Kunming Institute of Zoology, Chinese Academy of Sciences, Kunming, Yunnan 650223, China; Kunming College of Life Science, University of Chinese Academy of Sciences, Kunming 650204 Yunnan, China*

Chenglu He − *Department of Clinical Laboratory, First Affiliated Hospital of Kunming Medical College, Kunming 650032 Yunnan, China*

Ya Li − *Department of Clinical Laboratory, First Affiliated Hospital of Kunming Medical College, Kunming 650032 Yunnan, China*

Xiangsheng Liu − *Zhejiang Cancer Hospital, Hangzhou Institute of Medicine (HIM), Chinese Academy of Sciences, Hangzhou 310022 Zhejiang, China*

Xingyu Jiang − *Department of Biomedical Engineering, Southern University of Science and Technology, Shenzhen*

https://doi.org/10.1021/acs.nanolett.3c03909
Nano Lett. 2023, 23, 11874−11883

518055 Guangdong, China; orcid.org/0000-0002-5008-4703

Peter Muiruri Kamau − *Engineering Laboratory of Peptides of Chinese Academy of Sciences, Key Laboratory of Bioactive Peptides of Yunnan Province, KIZ-CUHK Joint Laboratory of Bioresources and Molecular Research in Common Diseases, National Resource Center for Non-Human Primates, National Research Facility for Phenotypic & Genetic Analysis of Model Animals (Primate Facility), and Sino-African Joint Research Center, New Cornerstone Science Institute, Kunming Institute of Zoology, Chinese Academy of Sciences, Kunming, Yunnan 650223, China; Kunming College of Life Science, University of Chinese Academy of Sciences, Kunming 650204 Yunnan, China*

Complete contact information is available at: https://pubs.acs.org/10.1021/acs.nanolett.3c03909

Author Contributions

[¶]Z.Z., Y.C., J.G., and M.Y. contributed equally to this work.

Notes

The authors declare no competing financial interest.

■ ACKNOWLEDGMENTS

This work was supported by the National Natural Science Foundation of China (32070443 and 21761142002), Chinese Academy of Sciences (XDB31000000, SAJC201606, KFJ-BRP-008, and KGFZD-135-17-011), and Yunnan Province Grant (202302AA310015).

■ REFERENCES

(1) Adedeji, W. A. The Treasure Called Antibiotics. *Annals of Ibadan Postgraduate Medicine* **2016**, *14* (2), 56−57.
(2) Costa, F.; Teixeira, C.; Gomes, P.; Martins, M. C. L. Clinical Application of AMPs. *Advances in experimental medicine and biology* **2019**, *1117*, 281−298.
(3) de Kraker, M. E. A.; Stewardson, A. J.; Harbarth, S. Will 10 Million People Die a Year due to Antimicrobial Resistance by 2050? *PLOS Medicine* **2016**, *13* (11), No. e1002184.
(4) Miller, L. G.; Perdreau-Remington, F.; Rieg, G.; Mehdi, S.; Perlroth, J.; Bayer, A. S.; Tang, A. W.; Phung, T. O.; Spellberg, B. Necrotizing Fasciitis Caused by Community-Associated Methicillin-Resistant Staphylococcus aureus in Los Angeles. *New England Journal of Medicine* **2005**, *352* (14), 1445−1453.
(5) Levin, A. S.; Barone, A. A.; Penço, J.; Santos, M. V.; Marinho, I. S.; Arruda, E. A. G.; Manrique, E. I.; Costa, S. F. Intravenous Colistin as Therapy for Nosocomial Infections Caused by Multidrug-Resistant Pseudomonas aeruginosa and Acinetobacter baumannii. *Clinical Infectious Diseases* **1999**, *28* (5), 1008−1011.
(6) Foster, T. J.; Geoghegan, J. A.; Ganesh, V. K.; Hook, M. Adhesion, invasion and evasion: the many functions of the surface proteins of Staphylococcus aureus. *Nature reviews. Microbiology* **2014**, *12* (1), 49−62.
(7) DeLeo, F. R.; Otto, M.; Kreiswirth, B. N.; Chambers, H. F. Community-associated meticillin-resistant Staphylococcus aureus. *Lancet* **2010**, *375* (9725), 1557−68.
(8) Otto, M. Basis of virulence in community-associated methicillin-resistant Staphylococcus aureus. *Annu. Rev. Microbiol.* **2010**, *64*, 143−62.
(9) Chambers, H. F.; Deleo, F. R. Waves of resistance: Staphylococcus aureus in the antibiotic era. *Nature reviews. Microbiology* **2009**, *7* (9), 629−41.
(10) DeLeo, F. R.; Chambers, H. F. Reemergence of antibiotic-resistant Staphylococcus aureus in the genomics era. *J. Clin. Invest.* **2009**, *119* (9), 2464−74.
(11) Wang, G.; Li, X.; Wang, Z. APD3: the antimicrobial peptide database as a tool for research and education. *Nucleic Acids Res.* **2016**, *44* (D1), D1087−D1093.
(12) Falanga, A.; Lombardi, L.; Franci, G.; Vitiello, M.; Iovene, M. R.; Morelli, G.; Galdiero, M.; Galdiero, S. Marine Antimicrobial Peptides: Nature Provides Templates for the Design of Novel Compounds against Pathogenic Bacteria. *Int. J. Mol. Sci.* **2016**, *17* (5), 785.
(13) Lombardi, L.; Falanga, A.; Del Genio, V.; Galdiero, S. A New Hope: Self-Assembling Peptides with Antimicrobial Activity. *Pharmaceutics* **2019**, *11* (4), 166.
(14) Han, Y.; Zhang, M.; Lai, R.; Zhang, Z. Chemical modifications to increase the therapeutic potential of antimicrobial peptides. *Peptides* **2021**, *146*, 170666.
(15) Mwangi, J.; Hao, X.; Lai, R.; Zhang, Z. Y. Antimicrobial peptides: new hope in the war against multidrug resistance. *Zoological research* **2019**, *40* (6), 488−505.
(16) Nordstrom, R.; Malmsten, M. Delivery systems for antimicrobial peptides. *Adv. Colloid Interface Sci.* **2017**, *242*, 17−34.
(17) Rai, A.; Pinto, S.; Velho, T. R.; Ferreira, A. F.; Moita, C.; Trivedi, U.; Evangelista, M.; Comune, M.; Rumbaugh, K. P.; Simões, P. N.; Moita, L.; Ferreira, L. One-step synthesis of high-density peptide-conjugated gold nanoparticles with antimicrobial efficacy in a systemic infection model. *Biomaterials* **2016**, *85*, 99−110.
(18) Wadhwani, P.; Heidenreich, N.; Podeyn, B.; Burck, J.; Ulrich, A. S. Antibiotic gold: tethering of antimicrobial peptides to gold nanoparticles maintains conformational flexibility of peptides and improves trypsin susceptibility. *Biomaterials science* **2017**, *5* (4), 817−827.
(19) Bi, L.; Yang, L.; Narsimhan, G.; Bhunia, A. K.; Yao, Y. Designing carbohydrate nanoparticles for prolonged efficacy of antimicrobial peptide. *Journal of controlled release: official journal of the Controlled Release Society* **2011**, *150* (2), 150−6.
(20) Brandelli, A. Nanostructures as promising tools for delivery of antimicrobial peptides. *Mini reviews in medicinal chemistry* **2012**, *12* (8), 731−41.
(21) Yang, X.; Yang, M.; Pang, B.; Vara, M.; Xia, Y. Gold Nanomaterials at Work in Biomedicine. *Chem. Rev.* **2015**, *115* (19), 10410−88.
(22) Ghosh, P.; Han, G.; De, M.; Kim, C. K.; Rotello, V. M. Gold nanoparticles in delivery applications. *Advanced drug delivery reviews* **2008**, *60* (11), 1307−15.
(23) Ben Haddada, M.; Blanchard, J.; Casale, S.; Krafft, J. M.; Vallee, A.; Methivier, C.; Boujday, S. Optimizing the immobilization of gold nanoparticles on functionalized silicon surfaces: amine- vs thiol-terminated silane. *Gold Bull.* **2013**, *46* (4), 335−341.
(24) Kumar, A.; Mandal, S.; Selvakannan, P. R.; Pasricha, R.; Mandale, A. B.; Sastry, M. Investigation into the Interaction between Surface-Bound Alkylamines and Gold Nanoparticles. *Langmuir: the ACS journal of surfaces and colloids* **2003**, *19* (15), 6277−6282.
(25) Hancock, R. E.; Sahl, H. G. Antimicrobial and host-defense peptides as new anti-infective therapeutic strategies. *Nature biotechnology* **2006**, *24* (12), 1551−7.
(26) Zhou, J.; Beattie, D. A.; Ralston, J.; Sedev, R. Colloid stability of thymine-functionalized gold nanoparticles. *Langmuir: the ACS journal of surfaces and colloids* **2007**, *23* (24), 12096−103.
(27) Bobone, S.; Stella, L. Selectivity of Antimicrobial Peptides: A Complex Interplay of Multiple Equilibria. *Advances in experimental medicine and biology* **2019**, *1117*, 175−214.
(28) Flemming, H. C.; Wingender, J. The biofilm matrix. *Nature reviews. Microbiology* **2010**, *8* (9), 623−33.
(29) Stewart, P. S.; Costerton, J. W. Antibiotic resistance of bacteria in biofilms. *Lancet* **2001**, *358* (9276), 135−138.
(30) Bjarnsholt, T. The role of bacterial biofilms in chronic infections. *APMIS. Supplementum* **2013**, *121*, 1−58.
(31) Allison, K. R.; Brynildsen, M. P.; Collins, J. J. Metabolite-enabled eradication of bacterial persisters by aminoglycosides. *Nature* **2011**, *473* (7346), 216−20.

(32) Maisonneuve, E.; Gerdes, K. Molecular mechanisms underlying bacterial persisters. *Cell* **2014**, *157* (3), 539−48.
(33) Chapple, D. S.; Mason, D. J.; Joannou, C. L.; Odell, E. W.; Gant, V.; Evans, R. W. Structure-function relationship of antibacterial synthetic peptides homologous to a helical surface region on human lactoferrin against Escherichia coli serotype O111. *Infection and immunity* **1998**, *66* (6), 2434−40.
(34) Ganewatta, M. S.; Chen, Y. P.; Wang, J.; Zhou, J.; Ebalunode, J.; Nagarkatti, M.; Decho, A. W.; Tang, C. Bio-inspired resin acid-derived materials as anti-bacterial resistance agents with unexpected activities. *Chemical Science* **2014**, *5* (5), 2011−2016.
(35) Kim, W.; Zou, G.; Hari, T. P. A.; Wilt, I. K.; Zhu, W.; Galle, N.; Faizi, H. A.; Hendricks, G. L.; Tori, K.; Pan, W.; Huang, X.; Steele, A. D.; Csatary, E. E.; Dekarske, M. M.; Rosen, J. L.; Ribeiro, N. d. Q.; Lee, K.; Port, J.; Fuchs, B. B.; Vlahovska, P. M.; Wuest, W. M.; Gao, H.; Ausubel, F. M.; Mylonakis, E. A selective membrane-targeting repurposed antibiotic with activity against persistent methicillin-resistant Staphylococcus aureus. *Proc. Natl. Acad. Sci. U. S. A.* **2019**, *116* (33), 16529−16534.
(36) Seelig, J.; Seelig, A. Lipid conformation in model membranes and biological membranes. *Q. Rev. Biophys.* **1980**, *13* (1), 19−61.
(37) Soo Choi, H.; Liu, W.; Misra, P.; Tanaka, E.; Zimmer, J. P.; Itty Ipe, B.; Bawendi, M. G.; Frangioni, J. V. Renal clearance of quantum dots. *Nature biotechnology* **2007**, *25* (10), 1165−1170.

https://doi.org/10.1021/acs.nanolett.3c03909
Nano Lett. 2023, 23, 11874−11883